ISSN 0018-1439, High Energy Chemistry, 2023, Vol. 57, Suppl. 1, pp. S137–S140. © Pleiades Publishing, Ltd., 2023.

Dependence of the Mechanical Properties of Porous Titanium Nickelide on the Pore Morphology under Compression

G. A. Nikiforov[a], *, B. N. Galimzyanov[a], and A. V. Mokshin[a]

[a] *Kazan Federal University, Kazan, Russia*

**e-mail: nikiforov121998@mail.ru*

Received April 10, 2023; revised April 10, 2023; accepted April 10, 2023

Abstract—Porous materials are widely used in many industries. However, their mechanical properties are inferior to those of their homogeneous non-porous analogues. In the present work, on the example of porous titanium nickelide, we studied the effect of the structure of the solid framework on the mechanical properties of the porous material. A method to improve the mechanical properties by achieving a uniform density profile along the strain direction is considered. It is shown that the uniform distribution of the crystalline matrix along the strain axis does not significantly affect on the mechanical properties of the porous system. The mechanism of pore collapse under compression has been investigated.

DOI: 10.1134/S0018143923070287

INTRODUCTION

The physical and mechanical properties of porous materials differ significantly from the properties of non-porous materials. Porous materials have relatively higher lightness, good sound insulation, catalytic capacity, and damping properties [1]. For this reason, porous materials are actively used in the aircraft industry to lighten the fuselage and wings of airplanes [2]. Due to the increased specific surface area, materials with an open porous structure can be used as radiators operating under high pressure blowing [3]. Porous materials also have applications as impact energy absorbers, for example their high damping properties are well suited as support materials for aircraft and rocket engines [4, 5]. Moreover, porous materials are actively used in medicine in the manufacture of implants that can be saturated with medications [6–8]. One of the most commonly used materials for implants is titanium nickelide (NiTi) due to its excellent biocompatibility and high elastic and plastic properties [9–11]. In particular, titanium nickelide has a superelasticity effect based on the martensitic transformation [12]. First-order phase transition between two basic crystalline phases: martensite (low-temperature) and austenite (high-temperature). However, porous materials have the obvious problem of deteriorating strength properties with increasing degree of porosity. For example, the Young's modulus decreases rapidly with increasing porosity of the material [13, 14]. In [15], data are given which indicate that the Young's modulus decreases with increasing pore size. For example, it was shown in [16] that with the same values of porosity, the Young's modulus is higher in samples with spherical pores than in samples with cylindrical pores. This raises the issue of improving the strength properties of porous NiTi without losing its useful functional properties. Obviously, the use of methods of alloying with other metals or changing the proportion of the initial components of the alloy does not allow to solve this issue. Therefore, one way to solve this problem is to change the morphology of the crystalline framework [17, 18]. In the present work, the influence of the morphology of the crystalline framework on the strength properties of the system on the example of porous NiTi is investigated by molecular dynamics simulation. The case of uniaxial compression is considered.

SIMULATION DETAILS

To obtain porous NiTi samples with the crystalline matrix, an original algorithm was developed to generate a porous structure with specified porosity and configurable pore sizes. The pore shape is approximated by an ellipsoid. The values of the semi-axes of the ellipsoid are chosen randomly from a given range of values. In this work, the range of ellipsoid semi-axis values is 2–6 nm. The developed algorithm can form a crystalline framework with a uniform density profile. The density profile is a graph of the density dependence of a layer on its coordinate along the selected direction. Using this algorithm, samples with a uniform pore distribution along the Ox axis and samples with a random distribution at average porosity values of 22.5, 38.5, and 58% were prepared based on the NiTi crystal system in the B2 phase. The simulation cell is cubic with an average linear size of 10 nm. The

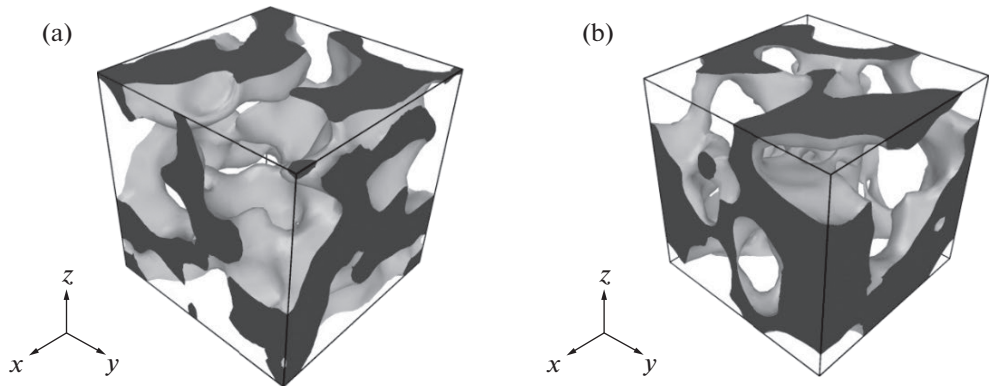

Fig. 1. Snapshots of porous samples: with a uniform density profile (a) and a non-uniform density profile (b) with porosity values of 58.0%.

interatomic potential is the second nearest-neighbor modified embedded atom method (2NN MEAM) [19]. All simulation steps were implemented in compliance with periodic boundary conditions. Each sample was subjected to uniaxial compression along the Ox axis at a strain rate of 5×10^9 c^{-1}. Compression was carried out to a strain $\varepsilon_{max} = 30\%$ in the NPT ensemble at 300 K and atmospheric pressure.

DISCUSSION RESULTS

Figure 1 shows some of the obtained porous systems. At a porosity value of 22.5%, the pores are closed spaces with rare overlap in both types of density profiles. At a porosity of 38.5%, there is frequent pore overlap. At 58% porosity, percolation is present in the system.

The difference in density profiles for samples with similar porosity but different pore distributions is shown in Fig. 2a. Samples with a uniform density profile have a uniform pore distribution along the corresponding direction, while samples with annon-uniform density profile have a random pore distribution. Compression causes the collapse of the pores during compaction of porous samples. Three main types of collapse were observed: pore collapse in areas of local minimums of the density profile (Fig. 2b), pore collapse in areas of local maximums of the density profile (Fig. 2c), and uniform compaction (Fig. 2d). It is detected that the samples with non-uniform density profile are characterized by collapse in the region of local minimums, and the samples with uniform density profile are characterized by collapse in the region of local maximums and uniform compression. It is also noted that a slight collapse in one of the local maximums can be observed during uniform compression (Fig. 2d).

Compressive stress-strain diagrams were calculated for different values of porosity (Fig. 3). The stepped shape of the stress-strain diagram for samples with a porosity of 22.5% (Fig. 3a) is caused by a change in the shape of the crystal grains. The stress decrease in the strain region of 23–27% is explained by the merging of crystalline grains with different orientations into a single crystallite. Due to their merger, the excess potential energy of the crystal lattice transfers heat, which causes the temperature to increase (Fig. 3d). The consequence of this is a decrease in stress in the material. The absence of other areas of mechanical stress decrease in samples with different porosity indicates that in places of material compaction (Fig. 2b) pore collapse occurs uniformly without destroying the crystalline matrix of the material. This is explained by the high value of surface tension at average pore sizes of the order of 5 nm, which provides pore stability at high stresses, as well as by the high plasticity of titanium nickelide.

Figure 4 shows the dependence of Young's modulus, elastic limit, and maximum achieved stress on porosity calculated for uniform and non-uniform density profile samples. The dependence of Young's modulus, elastic limit, and porosity for samples with non-uniform density profiles is approximated by the Balshin's [20] power dependence (Eqs. (3), (4)), and the dependence of maximum stress in the 30% strain range on porosity is approximated by the Duckworth's exponential dependence [21] (Eq. (5)):

$$E = E_0\left(1 - \frac{\phi}{100\%}\right)^n, \quad (3)$$

$$\sigma_{el} = \sigma_{el_0}\left(1 - \frac{\phi}{100\%}\right)^n, \quad (4)$$

$$\sigma_{max} = \sigma_{max_0} e^{\left(-\frac{b\phi}{100\%}\right)}. \quad (5)$$

As a limiting case for the dependencies considered, a crystalline sample without pores was prepared and subjected to compression under the same conditions. The corresponding mechanical characteristics for the specimen without pores are $E_0 = 137.5$ GPa, $\sigma_{el_0} = 4.6$ GPa and $\sigma_{max_0} = 58.4$ GPa.

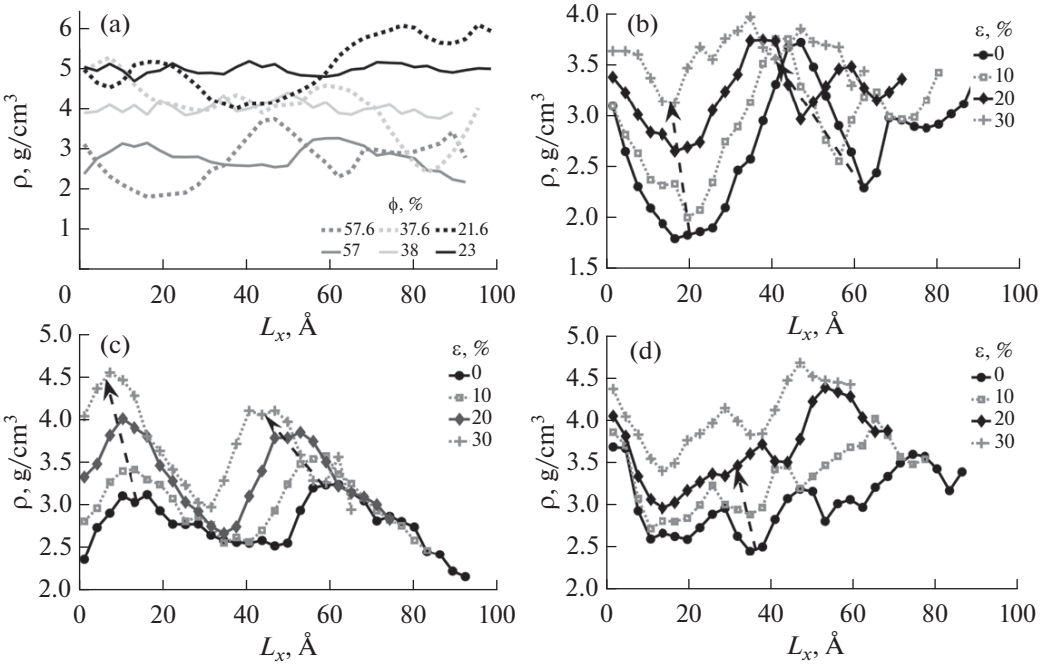

Fig. 2. Density profiles of some obtained samples. In panel (a) the solid line corresponds to a uniform pore distribution, and the dashed line corresponds to a random pore distribution. Panels (b), (c), (d) show the density profiles of porous systems with an average porosity of 58% in compression.

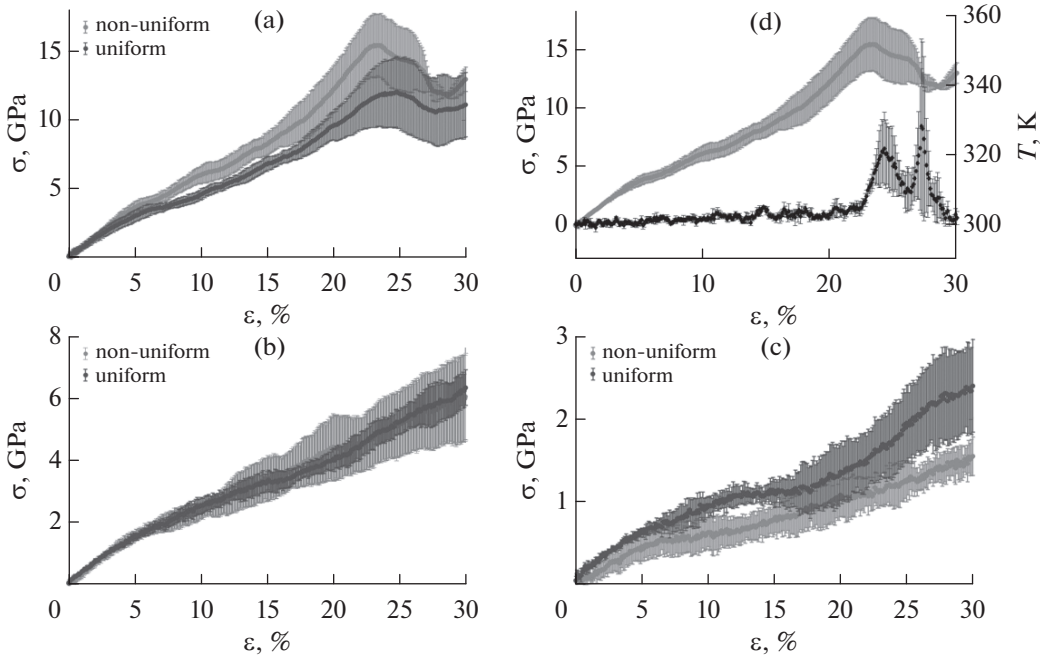

Fig. 3. Strain-stress curves for samples with porosity of 22.5% (a), 38.5% (b) and 58% (c). In panel (d), the stress-strain and temperature-strain curves are correlated.

The corresponding parameters $n = 2.78$ and $b = 6.3$ were calculated for porous titanium nickelide based on the obtained simulation data. Figures 4a and 4b shows that the data for the uniform distribution are also well described by the selected dependence with the specified value of n. This indicates that there is no pronounced dependence of the considered properties on the character of the density profile. It also follows from

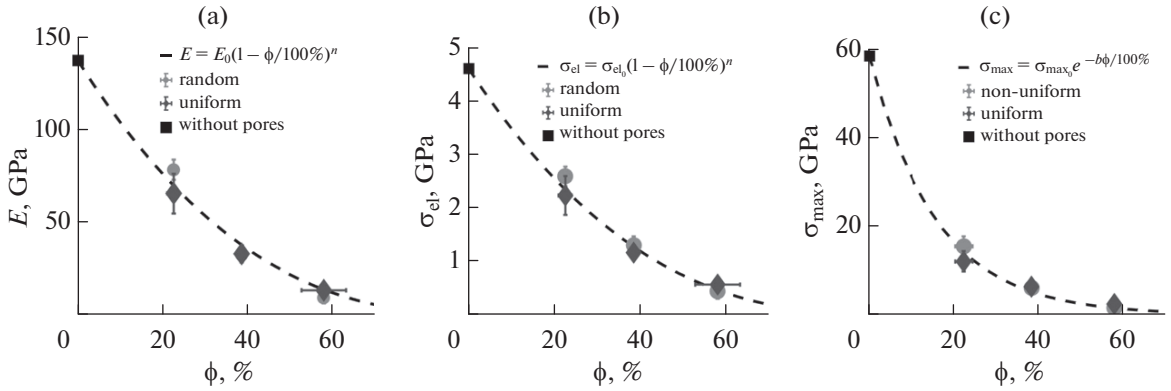

Fig. 4. Dependence of Young's modulus E (a), elastic limit σ_{el} (b) and maximum stress in the deformation section up to 30% σ_{max} (c) of porous NiTi on porosity.

graph 4c that the maximum stress does not depend on the character of the density profile. It is important to note that the application of machine learning methods [22] on large data sets containing different parameters of the morphology of the porous structure (pore size, pore shape, etc.) can reveal hidden dependencies not considered in this work.

CONCLUSIONS

In the course of this research it was shown that pore collapse occurs during compression without material failure. Three main types of pore collapse were identified: collapse in the zone of local minimum and maximum of the density profile and uniform compaction. The non-uniform density profile is characterized by collapse in the zone of local minimums of the density profile, and the uniform density profile is characterized by collapse in the zone of local maximums and uniform compression. It is shown that the distribution of pores in a porous sample does not affect the basic mechanical characteristics of the porous system in compression.

FUNDING

This study is supported by the Russian Science Foundation (project no. 19–12-00022).

CONFLICT OF INTEREST

The authors declare that they have no conflicts of interest.

REFERENCES

1. Liu, P.S. and Chen, G.F., *Porous Materials: Processing and Applications*, Amsterdam: Elsevier/Butterworth–Heinemann, 2014.
2. Davies, G.J. and Zhen, S., *J. Mater. Sci.*, 1983, vol. 18, p. 1899.
3. Xi, Z., Zhu, J., Tang, H., Ao, Q., Zhi, H., Wang, J., and Li, C., *Materials*, 2011, vol. 4, no. 4, p. 816.
4. Lu, T.J., He, D.P., and Chen, C.Q., *Adv Mech.*, 2006, vol. 36, no. 4, p. 517.
5. Chen, W.G. and Zhang, Q., *Powder Met. Ind.*, 2005, vol. 15, no. 2, p. 38.
6. Guden, M., Celik, E., and Cetiner, S., *Adv. Exp. Med. Biol.*, 2004, vol. 553, p. 257.
7. Wang, C.K., Wang, W.Y., Robert, F.M., et al., *J. Biomed. Mater. Res., Part B*, 2010, vol. 93. No. 2, p. 562.
8. Volchkov, S.E., Shishkovsky, I.V., and Bayrikov, I.M., *Cell Transplant. Tissue Eng.*, 2013, vol. 8, p. 52.
9. Duerig, T., Pelton, A., and Stockel, D., *Mater. Sci. Eng.*, 1999, vol. 273, p. 149.
10. Kapoor, D., *Johns. Matthey Technol. Rev.*, 2017, vol. 61, p. 66.
11. Shabalovskaya, S.A., *Bio-Med. Mater. Eng.*, 2002, vol. 12, p. 69.
12. Hartl, D.J. and Lagoudas, D.C., *Proc. Inst. Mech. Eng. G: Aerosp. Eng.*, 2007, vol. 221, p. 540.
13. Dean, E.A. and Lopez, J.A., *J. Am. Ceram. Soc.*, 1983, vol. 66, no. 5, p. 366.
14. Galimzyanov, B.N. and Mokshin, A.V., *Int. J. Solids Struct.*, 2021, vol. 224, p. 111047.
15. Kolesnikova, A.S., *Proceedings of SPIE*, vol. 10069: *Reporters, Markers, Dyes, Nanoparticles, and Molecular Probes for Biomedical Applications IX*, Achilefu, S. and Raghavacharti, R., Eds., San Francisco: SPIE, 2017, p. 4.
16. Carmen, T.-S., John, M., and Ross, B., *J. Mater. Eng. Perform.*, 2018, vol. 22, no. 6, p. 2901.
17. Tsygankov, A.A., Galimzyanov, B.N., and Mokshin, A.V., *J. Phys.: Condens. Matter*, 2022, vol. 34, no. 41, p. 414003.
18. Galimzyanov, B.N., Nikiforov, G.A., and Mokshin, A.V., *Acta Phys. Pol., A*, 2020, vol. 137, p. 1149.
19. Ko, W.-S., Grabowski, B., and Neugebauer, J., *Phys. Rev. B: Condens. Matter*, 2015, vol. 92, p. 134107.
20. Bal'shin, M.Yu., *Dokl. Akad. Nauk*, 1949, vol. 67, no. 5, p. 831.
21. Duckworth, W.H., *J. Am. Ceram. Soc.*, 1951, vol. 34, p. 1.

SPELL: 1. OK